NASA Technical Memorandum 107283
AIAA–96–2823

Experimental Investigation of Unsteady Flows at Large Incidence Angles in a Linear Oscillating Cascade

Daniel H. Buffum
Lewis Research Center
Cleveland, Ohio

Vincent R. Capece and Aaron J. King
University of California
Davis, California

Yehia M. EL-Aini
Pratt & Whitney
West Palm Beach, Florida

Prepared for the
32nd Joint Propulsion Conference
cosponsored by AIAA, ASME, SAE, and ASEE
Lake Buena Vista, Florida, July 1–3, 1996

National Aeronautics and
Space Administration

Experimental Investigation of Unsteady Flows at Large Incidence Angles in a Linear Oscillating Cascade

Daniel H. Buffum
NASA Lewis Research Center
Cleveland, Ohio U.S.A

Vincent R. Capece and **Aaron J. King**
Department of Mechanical & Aeronautical Engineering
University of California
Davis, California U.S.A

Yehia M. EL-Aini
Pratt & Whitney
West Palm Beach, Florida U.S.A

ABSTRACT

The aerodynamics of a cascade of airfoils oscillating in torsion about the midchord is investigated experimentally at a large mean incidence angle and, for reference, at a low mean incidence angle. The airfoil section is representative of a modern, low aspect ratio, fan blade tip section. Time-dependent airfoil surface pressure measurements were made for reduced frequencies up to 0.8 for out-of-phase oscillations at Mach numbers up to 0.8 and chordal incidence angles of 0° and 10°. For the 10° chordal incidence angle, a separation bubble formed at the leading edge of the suction surface. The separated flow field was found to have a dramatic effect on the chordwise distribution of the unsteady pressure. In this region, substantial deviations from the attached flow data were found with the deviations becoming less apparent in the aft region of the airfoil for all reduced frequencies. In particular, near the leading edge the separated flow had a strong destabilizing influence while the attached flow had a strong stabilizing influence.

NOMENCLATURE

C	blade chord length
C_M	first harmonic unsteady aerodynamic moment coefficient, Eq. 4
$\overline{C_p}$	steady pressure coefficient, $(p_{in} - p)/(\rho V^2)$
C_p	first harmonic unsteady pressure coefficient, $p_1/\rho V^2 \alpha_1$
Im	Imaginary part
k	reduced frequency, $\omega C/V$
M	inlet mach number
n	airfoil number 0, ±1, ... ±4
p_{in}	cascade mean inlet pressure
p_{ex}	cascade mean exit pressure
p	mean pressure (zeroth harmonic)
p_1	first harmonic unsteady pressure
Re	real part
Re_C	Reynolds number, $\rho VC/\mu$
R_p	cascade pressure ratio, p_{ex}/p_{in}
S	blade spacing
t_{max}	maximum blade thickness
V	inlet velocity
x	chordal distance
x_{max}	position of maximum blade thickness
x_p	pitching axis location
α	mean incidence relative to the airfoil chord-line
α_1	amplitude of torsional oscillation; $\alpha_1 = 0.0209$ radian
β	interblade phase angle
γ	stagger angle
θ^*	leading edge camber angle
μ	dynamic viscosity at cascade inlet
ρ	density at cascade inlet

ϕ phase angle

ω frequency of oscillation

INTRODUCTION

The demand for gas turbine engines with higher thrust-to-weight ratio and increased durability has made the structural dynamic response of fan and compressor blade rows due to blade flutter a problem of increasing concern. In particular, as part of the engine design process, blade flutter must be accurately predicted. The failure to accurately account for this phenomenon can lead to premature engine failure and reduced engine life.

Many different types of flutter can occur in turbomachines; Fig. 1 illustrates the flutter regions on a compressor performance map. Subsonic/transonic stall flutter, schematically depicted near the stall line at part speed, is the most difficult type of flutter to accurately predict because viscous effects are significant. Current state-of-the-art unsteady viscous codes have not been demonstrated to provide accurate predictions of stall flutter at high incidence and transonic relative inlet Mach numbers. As a result, current stall flutter prediction systems rely on purely empirical correlations of flutter boundaries based on previous rig and engine testing, simplified separation models, or semi-empirical methods.[1]

To evaluate current unsteady aerodynamic models and direct the development of future models, experimental data from oscillating cascade experiments are required. It is extremely difficult to obtain valid experimental data with the reduced frequency, Mach number, and mean incidence simultaneously having appropriate values. In addition, data for simultaneous oscillation of the airfoils at a number of different interblade phase angles is desirable. Hence, there is a very limited quantity of cascade unsteady aerodynamic data appropriate for understanding and prediction of stall flutter.

Carta and St. Hilaire[2] and Carta[3], measured the surface chordwise unsteady pressure distribution on harmonically oscillating NACA 65 Series airfoils in a linear cascade. These torsionally oscillated airfoils exhibited a decrease in aerodynamic damping for increased incidence angles even though the steady suction surface static pressure distribution indicated attached flow. Although the interblade phase angles in these experiments were within the range found for stall flutter, the Mach number (< 0.2) and reduced frequency (0.4 based on chord) values were low.

Szechenyi and Finas[4] and Szechenyi and Girault[5] obtained unsteady aerodynamic data over a range of Mach numbers, reduced frequencies, and incidence angles, including partially and fully separated flow for a symmetrical airfoil harmonically oscillating in torsion. For 0.5 inlet Mach number, experimental results indicated negative aerodynamic damping for incidence angles greater than 8 degrees for a reduced frequency of 0.74. In this experiment only one blade was oscillated, and the unsteady aerodynamic coefficients correspond to the influence of the oscillation of the reference blade on itself when all other blades in the cascade are fixed.

These previous investigations have been partially successful at obtaining appropriate data to improve stall flutter prediction capabilities. However, Buffum et al.[6] have recently performed experiments using the NASA Lewis Research Center Transonic Oscillating Cascade to obtain unsteady aerodynamic data in the appropriate parameter ranges. In these experiments, the steady and unsteady aerodynamics of a cascade of airfoils oscillating in torsion about the midchord were measured. The airfoil section was representative of a modern low aspect ratio fan blade. Chordal incidence angles of 0 and 10° were used. Unsteady chordwise surface pressure measurements were made at a Mach number of 0.5, reduced frequencies up to 1.2, and a Reynolds number of 0.9 million. For the large mean incidence angle, a separation bubble formed at the leading edge of the suction surface. The separated flow field was found to have a destabilizing influence in the leading edge region for the 180 degree interblade phase angle used in the study.

In this paper, the aerodynamics of a cascade of airfoils executing torsion mode oscillations is investigated for subsonic and transonic Mach numbers using the airfoil cross-section from Buffum et al.[6]. For an inlet Mach number of 0.2, results will be presented for a low mean incidence, attached flow condition and a high mean incidence condition with leading edge separation. Results are presented for a Mach number of 0.8 for the high mean incidence condition with leading edge separation. Low incidence angle data for this Mach number were not obtainable because the cascade choked at a Mach number of 0.7 at 0° chordal incidence. Additionally, some Mach 0.5 data will be used for comparison. For details concerning the Mach 0.5 data, see Reference 6. Reduced frequencies of 0.4 and 0.8 are presented. The low incidence data are correlated with predictions from a linearized cascade unsteady aerodynamics code.

FACILITY AND INSTRUMENTATION

Oscillating Cascade

The NASA Lewis Oscillating Cascade, Fig. 2, combines a linear cascade wind tunnel capable of inlet flow approaching Mach 1 with a high-speed airfoil drive system. The drive system imparts torsional oscillations to the cascaded airfoils at specified interblade phase angles and realistic values of reduced frequency. For facility details not discussed below, see Buffum and Fleeter[7].

Air drawn from the atmosphere passes though honeycomb into a smooth contraction inlet section then into a constant area rectangular duct. For an inlet Mach number of 0.2, turbulence intensity in the test section was 0.3%. The duct measures 9.78 cm in span and 58.6 cm along the stagger line. Upstream of the test section, suction is applied through perforated sidewalls to reduce the boundary layer thickness. Tailboards are used to adjust the cascade exit region static pressure and also form bleed scoops which further reduce upper and lower wall boundary layer effects. Downstream of the test section, the air is expanded through a diffuser into an exhaust header. The cascade inlet may be adjusted to obtain a wide range of incidence angles.

The facility features a high-speed mechanism which may drive any or all of the airfoils in controlled torsional oscillations. For this investigation, all the airfoils were oscillated simultaneously, and the maximum reduced frequency was 0.8 (based on chord). At an inlet Mach number of 0.8, this corresponds to a 370 Hz oscillation frequency. Stainless steel barrel cams, each having a six-cycle sinusoidal groove machined into its periphery, are mounted on a common rotating shaft driven by a 74.6 kW electric motor. A cam follower assembly, consisting of a titanium alloy connecting arm with a stainless steel button on one end, is joined on the other end to an airfoil trunnion. The button fits into the cam groove, thus coupling the airfoil with the camshaft. The drive system geometry fixes the pitching amplitude to 1.2°. Lubrication of the cam/follower assembly is provided by an oil bath. The interblade phase angle is fixed by the relative positions of the cams on the drive shaft.

External to the oil bath, on the same shaft as the airfoil drive cams, is a cam used to indicate the shaft position. A proximity probe facing this reference cam produced a time-dependent voltage indicating the position of the airfoils.

The upper wall and the lower tailboard are acoustically treated. Experiments performed before acoustic treatment was installed[8,9] indicated that reflections of acoustic waves by the solid walls were compromising the blade-to-blade periodicity of the unsteady flow field. Thus the walls were modified to reduce acoustic wave reflections. Portions of the solid boundaries were replaced by perforated plates backed by enclosures filled with Kevlar fiber as depicted in Fig. 3. Rice[10] provided the design parameters (plate thickness and porosity, hole diameter, enclosure depth and Kevlar density). Bleed lines were attached to the cavities to allow boundary layer suction through the perforated walls.

Airfoils

The airfoils used in this study have a cross-section similar to that found in the tip region of current low aspect ratio fan blades. The airfoil section was designed using the Pratt & Whitney fan and compressor aerodynamic design system, which is for flow in circular ducts. Hence, to simulate the two dimensional conditions to be encountered in the linear cascade, the airfoils were designed using a radius ratio of 0.99. The loading levels, losses, solidity, and stagger angle are consistent with current design practice for fan blades. The airfoil cascade parameters are given in Table 1; refer to Fig. 4 for definitions of the geometry.

Table 1 Airfoil and cascade parameters

Chord, C	8.89 cm
Maximum thickness, t_{max}	0.048 chord
Location of maximum thickness, x_{max}	0.625 chord
Leading edge camber angle, θ^*	-9.5 degrees
Number of airfoils	9
Stagger angle, γ	60 degrees
Solidity, C/S	1.52
Pitching axis	0.5 chord

Instrumentation

Wall static pressure taps were used to measure the inlet and exit pressures. From these measurements, mean values were determined to provide the cascade pressure rise.

Four airfoils were instrumented with static pressure taps. Two airfoils were instrumented with taps very near the midspan, one on the suction surface, the other on the pressure surface. As shown in Fig. 5(a), taps were clustered near the leading edge to capture the large pressure gradients there. Taps were also clustered in the 50 to 70% chord region in anticipation of shock wave impingement on the pressure surface when operating near choked flow conditions. Two additional airfoils were instrumented with pressure taps, Fig. 5(b), some of which are redundant to the midspan instrumentation shown in part (a) and others which indicate the spanwise variations in the pressure. The redundant midspan taps were used to indicate blade-to-blade periodicity of the cascade steady flow field. The spanwise taps supply information on the three-dimensionality of the flow field.

Two airfoils were instrumented with flush-mounted miniature pressure transducers. The transducers were chosen for having the following desirable characteristics: small dimensions, high frequency response and invariance of dynamic response with change in temperature. Static and dynamic calibrations were made.

Kulite Semiconductor Products miniature pressure transducers were used, each of which consists of a silicon diaphragm containing a four-arm strain gage bridge mounted over a cylindrical cavity. Slots were machined into the airfoil surfaces to allow the transducer diaphragms to be mounted flush with the airfoil surface and to serve as passages for the wire leads. Once the transducers were installed, each slot was filled and smoothed to the airfoil contour, and each transducer was coated with RTV (room-temperature-vulcanizing rubber) for improved durability and conformance with the airfoil profile. To provide isolation from airfoil strain, each transducer was potted in RTV. The pressure sensitive diameter was 0.7 mm (0.8% of the airfoil chord).

The transducers were located on the upper surface of one airfoil and the lower surface of another airfoil. There were 15 transducers per surface. The locations, the same as those of the midspan pressure taps (Fig. 5(a)), vary from 6 to 95% of chord. The transducer thickness relative to the airfoil thickness was the limiting factor in placing the transducers closest to the leading and trailing edges; at these locations, the airfoil thickness was chosen to be at least twice the transducer thickness.

Static calibration of the transducers was performed at NASA Lewis Research Center. Each blade was installed in a calibration chamber, the ambient pressure of which was controlled using a vacuum pump. The transducer electronics and the data acquisition system were identical to those used during all of the calibrations and the unsteady experiments. The response for each transducer was linear. The calibrations were repeatable - changes in sensitivities were typically less than 0.25% between calibrations.

To determine the frequency response of the transducers, a resonant tube assembly similar to that used by Capece and Fleeter[11] was used to excite the transducers with acoustic waves. The assembly consists of a 20.3 cm diameter, 4.6 m long plastic tube with a speaker mounted at one end. An instrumented airfoil was mounted at the opposite end of the tube, which was open to atmosphere. Amplified sine waves were used to drive the speaker which in turn created acoustic waves in the tube for excitation of the transducers. The resulting pressure transducer responses were flat to frequencies in excess of 1000 Hz within ±2% in magnitude and ±3 degrees in phase.

During the experiments, the pressure transducers are subject to maximum accelerations in excess of 300 times that due to gravity. Acceleration deflects the transducer diaphragm and thus produces apparent pressure signals. Calibration was used to correct for this effect. Each blade was oscillated in a chamber with low ambient pressure (1.2 kPa) over the range of frequencies encountered in the experiments. The mode of oscillation was identical to that used in the cascade. Through Fourier analysis of the resulting signals, the transducer responses as a function of oscillation frequency were determined. Second degree polynomial curves were found to fit the calibration data well; the calibration coefficients were used to correct the experimental data. For example, at 370 Hz, the correction for the upper surface leading edge transducer was 2.6 kPa.

DATA ACQUISITION AND ANALYSIS

Unsteady signals from the pressure transducers and the proximity probe were recorded using a Teac XR-7000 VHS tape recorder. During tape playback, the signals were simultaneously digitized at rates typically 10 times the oscillation frequency, with 16,384 samples taken per channel. Each channel of data was divided into blocks with 1024 samples, windowed using a Hanning window, then Fourier transformed to determine the first harmonic of each block. The first harmonic of each block was referenced to the airfoil motion by subtracting from it the phase of the first harmonic motion signal (from the proximity probe) of the corresponding block. Once all of the blocks from a channel were decomposed in this manner, the first harmonic block results were averaged and the complex-valued acceleration response was subtracted vectorally.

The motion of the nth airfoil is defined by the change in the incidence angle with time:

$$\alpha^n(t) = \alpha + \alpha_1 Re[\exp(i(\omega t + n\beta))] \tag{1}$$

The first harmonic unsteady pressure coefficient is defined as

$$C_p(x) = \frac{p_1(x)}{\rho V^2 \alpha_1} \tag{2}$$

The pressure difference coefficient is defined to be the difference between the lower and upper surface unsteady pressure coefficients:

$$\Delta C_p = (C_p)_{lower} - (C_p)_{upper} \tag{3}$$

The unsteady aerodynamic moment coefficient for a flat plate airfoil is defined as

$$C_M = \int_0^1 \left(\frac{x_p}{C} - \frac{x}{C}\right)\Delta C_p\left(\frac{x}{C}\right) d\frac{x}{C} \tag{4}$$

$$= \int_0^1 C'_M \, d\frac{x}{C} \tag{5}$$

where $C'_M = \left(\frac{x_p}{C} - \frac{x}{C}\right)\Delta C_p\left(\frac{x}{C}\right)$ and x_p/C=0.5. The work done on the airfoil by the fluid per cycle of oscillation is proportional to $Im(C_M)$, thus the sign of $Im(C_M)$ determines the airfoil stability with $Im(C_M)$> 0 indicating instability.

RESULTS

Results will be presented for 0° and 10° of incidence at an inlet Mach number of 0.2 and for 10° incidence at 0.8 Mach number. These incidence angles are based on the cascade inlet angles relative to the airfoil chord-line; upstream flow angle measurements were not made. Unsteady data will be presented for a 180° interblade phase angle and reduced frequencies of 0.4 and 0.8.

For $\alpha = 0°$, the steady and unsteady data are correlated with two dimensional potential flow predictions; the influence of stream tube contraction was not considered in the analyses. For $\alpha = 10°$, solutions were not obtainable due to the extremely large flow gradients created by the sharp leading edge of the airfoils. The steady flow surface pressure distribution is correlated with the nonlinear full potential solver SFLOW[12], and the first harmonic surface pressure distribution is correlated with the linearized analysis LINFLO[13]. The predictions from SFLOW are used by LINFLO as the nonlinear background steady flow around which the harmonic unsteady flow solutions are formed.

The airfoil trailing edge was modified by inserting a wedge in place of the finite radius trailing edge for enforcement of the Kutta condition. This gave a trailing edge that was not a true cusp configuration. This was found to challenge the steady and unsteady computational implementations of the Kutta condition.

A 120 by 21 H-Grid was used in the computations. A localized region of the grid is illustrated in Fig. 6. This cosine distributed grid yields a large number of grid points in the leading and trailing edge regions where the flow gradients are the highest. The cascade inlet flow angle was varied until the best match was found between the steady chordwise pressure coefficient data and the predictions. This resulted in a 1.5° chordal incidence angle being used in all of the predictions.

Steady Aerodynamics

For a linear cascade to be a valid simulation of a turbomachine blade row, the cascade must exhibit good passage-to-passage periodicity for the steady flow field. To verify that the cascade was periodic, airfoil surface pressure distributions were obtained at the center airfoil position (position 0) and the two adjacent positions (positions -1 and 1) in the nine airfoil cascade. The resulting airfoil surface pressure distributions for M=0.2 and $\alpha = 0°$ are shown in Fig. 7. There is a net increase in the pressure coefficient through the passage which indicates that the flow is accelerating. Overall, the periodicity is good. From the leading edge to 30% of chord on the upper surface , the position 1 $\overline{C_p}$ values are somewhat larger that the rest. On the lower surface, the position -1 values tend to be less than the others, with the larger differences again being toward the leading edge. Cascade pressure ratio and Reynolds number for the steady flow conditions are given in Table 2.

There is excellent agreement between the data and the SFLOW predictions up to about 80% chord. Aft of this location the predictions show a steep pressure gradient as the trailing edge is approached, whereas the upper surface data do not have this trend and the lower surface data have a more gradual pressure gradient. The discrepancy in the data-theory correlation in this region is attributed to the airfoil modification and viscous effects. The predicted static pressure ratio for the cascade was 0.994.

Increasing the incidence angle to 10° (Fig. 8) changes the behavior of the cascade so that now there is flow separation off the leading edge of the airfoil upper surface and a net pressure rise across the cascade. Cascade periodicity is improved relative to the low incidence data.

Increasing the inlet Mach number to 0.8 while maintaining the 10° incidence angle (Fig. 9) does little to change the steady pressure coefficient distribution from that for M=0.2. Low incidence, M=0.8 data are not available because, at $\alpha = 0°$, the cascade choked at M=0.7.

To visualize the flow, the airfoil surface was coated with an oil-pigment mixture. At 10° incidence, separation from the upper surface was evident. The largest separated region was found at midspan; there, the flow was separated from the leading edge to about 40% of chord. Near the endwalls, the separation bubble extended to about 7% of chord. Between midspan and the endwalls, the reattachment region was defined by a smooth arc. This qualitative description is independent of inlet Mach number.

To quantify three-dimensional effects in the steady flow, pressure taps were placed at several different spanwise locations of the blade upper surface. Despite the three-dimensional nature of the separation bubble, Fig. 10 shows that the midspan and 35% span pressure distributions are nearly identical. Over the first half of the airfoil, the 17.5% span data for the upper surface differ from the other data. Clearly, this is due to the three-dimensional nature of the separated flow. The upper surface 17.5% span data with the peak near the leading edge and the rapid decrease in $\overline{C_p}$ with increasing chordwise position more closely resemble attached flow data, in contrast to the data at the other spanwise positions.

Table 2 Cascade pressure ratio and Reynolds number

Mach no.	Incidence	Pressure ratio	Reynolds number
0.2	0°	0.996	0.38×10^6
0.2	10°	1.006	0.38×10^6
0.8	10°	1.075	1.2×10^6

Unsteady Aerodynamics

Unsteady pressure data will be presented for out-of-phase oscillations ($\beta = 180°$). The $\alpha = 0°$ data will be correlated with linearized flow analysis predictions. Comparisons between the M=0.2 $\alpha = 0°$ and $\alpha = 10°$ data will be used to isolate effects of the mean flow on the unsteady aerodynamics. The effects of reduced frequency and Mach number on the unsteady separated flow will also be investigated. Cascade dynamic periodicity was a primary concern; to quantify periodicity, unsteady data were obtained at the center airfoil position and the two adjacent positions in the nine airfoil cascade.

Starting with the M=0.2 $\alpha = 0°$ data, first harmonic unsteady pressure coefficients for $\beta = 180°$, k=0.8 are shown in Fig. 11. Data were taken for three blade positions. Referring to the schematic in Fig. 11, data were taken at blade positions -1, 0 (the cascade center) and 1. For the C_p values, 95% confidence intervals of ±5% are estimated . For both surfaces, the data are highly periodic. The lower surface response is dominated by $Re(C_p)$ forward of midchord. Gaps in the lower surface data at 60 and 65% of chord are due to transducer failures. In contrast, the upper surface response on the forward half of the airfoil is nearly constant outside of an abrupt increase in both the real and imaginary parts very near the leading edge. As with the lower surface, data at some upper surface transducer locations are missing due to faulty transducers.

The predictions of the chordwise distribution of C_p are in good agreement with the data in both magnitude and trend.

Changing the mean incidence angle to 10° has a dramatic effect on the upper surface unsteady pressure coefficient distributions. The lower surface data, Fig. 12(a), are quite similar to the $\alpha = 0°$ data although the $Re(C_p)$ data reach a slightly smaller peak in the leading edge region. The upper surface pressure coefficients, Fig. 12(b), are affected significantly by the separation; relative to the $\alpha = 0°$ data, much larger pressure fluctuations are evident over the first half of the blade with the exception of x/C=0.06. Despite the severely separated flow, the unsteady pressure data are highly periodic.

Airfoil upper surface pressure spectra for these two conditions are shown in Fig. 13. At low incidence, Fig. 13(a), the spectra are dominated by the response at the oscillation frequency, and only in the measurement nearest the leading edge is there a significant higher harmonic response. In contrast, the high incidence spectra, Fig. 13(b), show higher harmonics at all locations encompassed by the steady flow separation bubble. However, the first harmonics are still dominant.

To further investigate mean flow effects, unsteady data were obtained for M=0.8, $\alpha = 10°$. C_p distributions for $\beta = 180°$, k=0.8 are shown in Fig. 14. The data generally exhibit good periodicity, although there are some blade-to-blade differences in the imaginary part where the flow was separated. The data are qualitatively quite similar to the M=0.2, $\alpha = 10°$ data, although the magnitudes of the C_p values on the lower surface are larger for the larger Mach number.

The effect of Mach number on ΔC_p distributions for $\alpha = 10°$ and k=0.8 is shown in Fig. 15 for M=0.2, 0.5 and 0.8. The ΔC_p values were calculated using the center airfoil data; where center airfoil data were incomplete, available data from the neighboring airfoils were used. The difference in magnitude for M=0.2 and 0.5 is small, but the values for M=0.8 are significantly larger. Phase differences are relatively small over the first half of the airfoil. Beyond that, the differences are much larger: at 80 and 90% of chord, the M=0.2 phase angle data differ from the corresponding M=0.5 and 0.8 data by roughly 100°.

Since the aeroelastician is ultimately interested in predicting the stability of a blade row, data illustrating the effect of the mean flow on the chordwise distribution of $Im(C'_M)$ are shown in Fig. 16. As discussed earlier, the work done by the fluid on the airfoil per cycle of oscillation is proportional to $Im(C'_M)$. For M=0.2 and 0.5, $Im(C'_M)$ data for both $\alpha = 0°$ and 10° are presented in addition to the M=0.8, $\alpha = 10°$ data. The most obvious differences are due to the gross nature of the flow, i.e., attached versus separated flow. In the vicinity of the leading edge, the attached flow contributes to the cascade stability while the separated flow is destabilizing. In a region varying from 8 to 16% of chord, the opposite becomes true: the attached flow is destabilizing and the separated flow in stabilizing. Beyond midchord, the trends become the same although the separated flow condition leads to a greater stabilizing influence than the attached flow.

On the basis of these data, increasing the Mach number appears to increase the cascade stability when the flow is separated. However, because the stability is strongly dependent on the unsteady aerodynamics near the airfoil leading edge, the question of the stability of this airfoil section cannot be definitively answered.

Fig. 17 shows the effect of reduced frequency on the chordwise distribution of $Im(C'_M)$ for M=0.8. Outside the leading edge region, the higher reduced frequency data indicate greater stability. Very near the leading edge, however, the k=0.8 curve has greater slope and potentially a greater destabilizing influence.

SUMMARY AND CONCLUSION

A series of fundamental experiments have been performed in the NASA Lewis Transonic Oscillating Cascade Facility to investigate the steady and torsion mode oscillating aerodynamics of both attached and separated flow for subsonic and transonic mean flow conditions, and realistic values of reduced frequency. For an inlet Mach number of 0.2, steady and unsteady aerodynamic data were presented for low mean incidence attached flow and high mean incidence flow with leading edge separation. The surface pressure distributions were quantified for reduced frequencies of 0.4 and 0.8. Additionally, for an inlet Mach number of 0.8 steady and unsteady aerodynamic data for the high mean incidence flow with leading edge separation were presented for reduced frequencies of 0.4 and 0.8. Low mean incidence data for this Mach number were not obtainable because the cascade choked at a Mach number of 0.7 for $\alpha = 0°$. For the attached flow cases the steady and unsteady aerodynamic data were correlated with potential flow analysis predictions.

Analysis of this data and correlation with predictions from the potential flow analysis indicate the following:

1) The steady mean flow was found to separate from the leading edge and reattach at 40% chord at 10 degrees of chordal incidence. While the separation zone was found to decrease in the endwall regions, the flow was shown to be two dimensional in the midspan region where the steady and unsteady aerodynamic response measurements were quantified.

2) The passage-to-passage periodicity was found to be good for attached and separated steady flow, signifying that the cascade provided a valid simulation of a turbomachinery blade row. The cascade also exhibited good passage-to-passage dynamic periodicity for attached and separated flow, thus providing a valid simulation of a turbomachine blade row undergoing torsion mode oscillations at a constant interblade phase angle.

3) Significant differences in the unsteady pressure distributions were found between attached and separated flow. In the separated flow regions, substantial deviations from attached flow, low incidence data were found with the deviations becoming less in the aft region of the airfoil.

4) Comparing the chordwise distribution of $Im(C'_M)$ forward of midchord revealed opposite trends for attached and separated flows. In the leading edge region, separated flows had a strong destabilizing influence whereas the attached flows had a strong stabilizing influence. Conversely, between 10 and 50% of chord, the separated flows become stabilizing while the attached flows became destabilizing. Aft of midchord, the differences were smaller. The destabilizing influence in the leading edge region for separated flow decreased with increasing Mach number. Additionally, for attached flow, increasing the Mach number was also found to be more stabilizing at the leading edge and also in the 20% chord region. These phenomena need further investigation.

5) For a Mach number of 0.8, the $Im(C'_M)$ distribution for separated flow indicated that an increasing reduced frequency might be more destabilizing in the immediated leading edge region. However, just downstream of the leading edge, increasing the reduced frequency had a strong stabilizing effect.

6) Correlation of the steady attached flow experimental data with the predictions from a nonlinear two dimensional potential code was good except in the trailing edge region. The discrepancy between the data and the predictions are attributed to viscous effects not included in the computational model and the replacement of the finite radius trailing edge with a wedge.

7) Correlation of the attached flow first harmonic data with predictions from a linearized potential code was good over most of the airfoil. The predictions captured the trend and magnitude of the unsteady pressure distributions. Differences between the experimental data and the predictions were most significant in the trailing edge region where the deviations in the steady flow were also influencing the unsteady predictions.

ACKNOWLEDGEMENT

Support of this research program by the NASA Lewis Research Center and Pratt & Whitney, Government Engines & Space Propulsion, is gratefully acknowledged. Dr. Daniel Hoyniak of Westinghouse Electric Corp. provided many helpful suggestions to improve the computational predictions. The successful completion of the experiments was enabled by excellent engineering and technical support. The engineers were W. Camperchioli, T. Jett, H. La, J. Little and V. Verhoff. The technicians were D. Costello, M. Lupica and R. Torres. Of particular importance were improvements made by Thomas Jett and Ricardo Torres which greatly reduced the down time for the frequent cascade configuration changes.

REFERENCES

[1]Capece, V.R., and EL-Aini, Y.M., "Stall Flutter Prediction Techniques for Fan and Compressor Blades," *Journal of Propulsion and Power*, Vol. 12, No. 3, May-June 1996.

[2]Carta, F.O. and St. Hilaire, A.O., "Effect of Interblade Phase Angle and Incidence Angle on Cascade Pitching Stability," ASME Paper No. 79-GT-153, 1979.

[3]Carta, F.O., "Unsteady Aerodynamics and Gapwise Periodicity of Oscillating Cascaded Airfoils," ASME *Journal of Engineering for Power*, Vol. 105, 1983, pp. 565-574.

[4]Széchényi, E. and Finas, R., "Aeroelastic Testing in a Straight Cascade Wind Tunnel," *Aeroelasticity in Turbomachines*, Edited by P. Suter, Juris-Verlag, 1981, pp. 143-149.

[5]Széchényi, E. and Girault, J.Ph., "A Study of Compressor Blade Stall Flutter in a Straight Cascade Wind Tunnel," *Aeroelasticity in Turbomachines*, Edited by P. Suter, Juris-Verlag, 1981, pp. 163-169.

[6]Buffum, D.H., Capece, V.R., King, A.J. and EL-Aini, Y.M., "Oscillating Cascade Aerodynamics at Large Mean Incidence," 1996, ASME Paper 96-GT-339.

[7]Buffum, D.H. and Fleeter, S., "Aerodynamics of a Linear Oscillating Cascade," NASA Technical Memorandum 103250, 1990.

[8]Buffum, D.H. and Fleeter, S., "Wind Tunnel Wall Effects in a Linear Oscillating Cascade," ASME *Journal of Turbomachinery*, Vol. 115, 1993, pp. 147-156.

[9]Buffum, D.H. and Fleeter, S., "Effect of Wind Tunnel Acoustic Modes on Linear Oscillating Cascade Aerodynamics," ASME *Journal of Turbomachinery*, Vol. 116, 1994, pp. 513-524.

[10]Rice, E.J., Private Communication, NASA Lewis Research Center, Cleveland, OH, 1992.

[11]Capece, V.R. and Fleeter, S., "Forced Response Unsteady Aerodynamics in a Multistage Compressor," Purdue University Report ME-TSPC-TR-87-12, 1987.

[12]Hoyniak, D. and Verdon J.M., "Development of a Steady Potential Solver for Use with Linearized Unsteady Aerodynamic Analyses," Unsteady Aerodynamics, Aeroacoustics, and Aeroelasticity of Turbomachines and Propellers, Edited by H.M. Atassi, Springer-Verlag, 1993, pp. 177-194.

[13]Verdon, J.M. and Hall, K.C., "Development of a Linearized Unsteady Aerodynamic Analysis for Cascade Gust Response Predictions," NASA Contractor Report NAS3-25425, 1990.

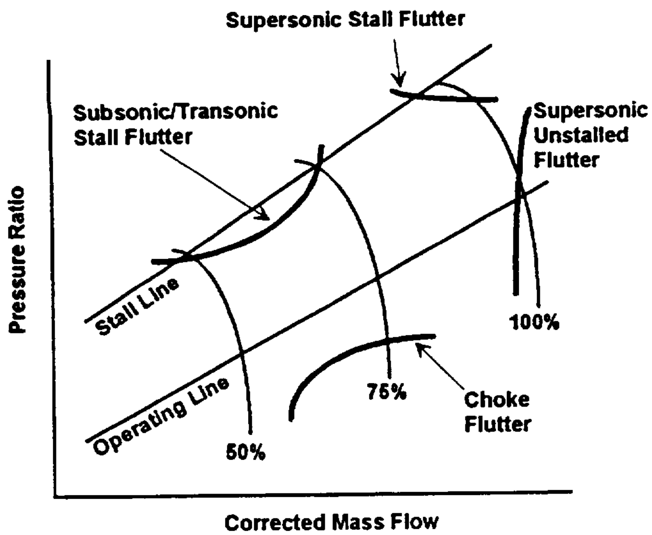

Fig.1 Compressor performance map showing flutter boundaries

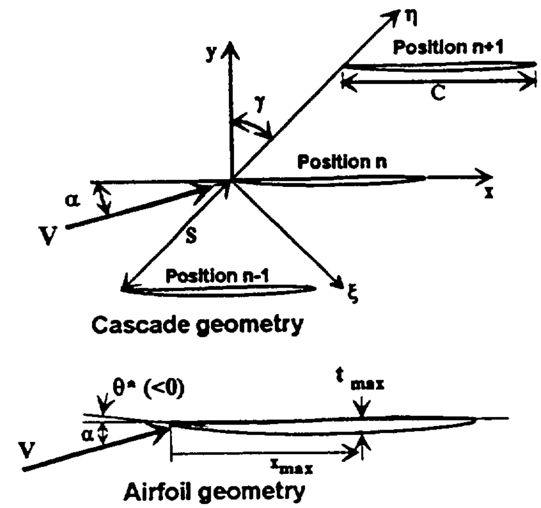

Fig. 4 Airfoil and cascade geometry

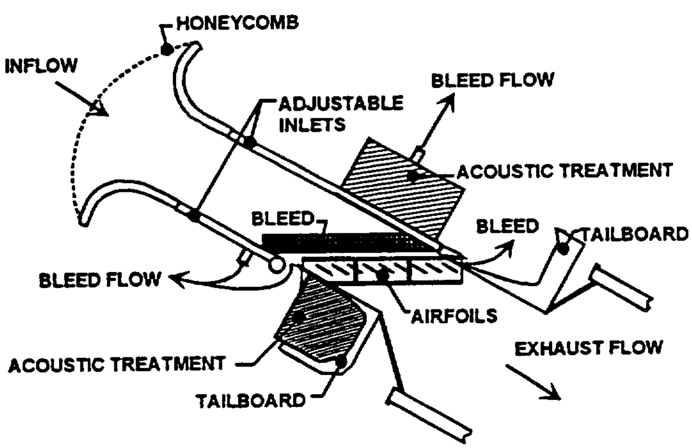

Fig. 2 NASA Lewis Oscillating Cascade

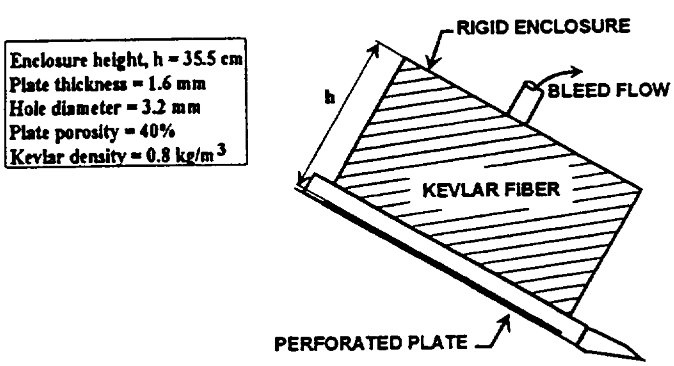

Fig. 3 Upper wall acoustic treatment

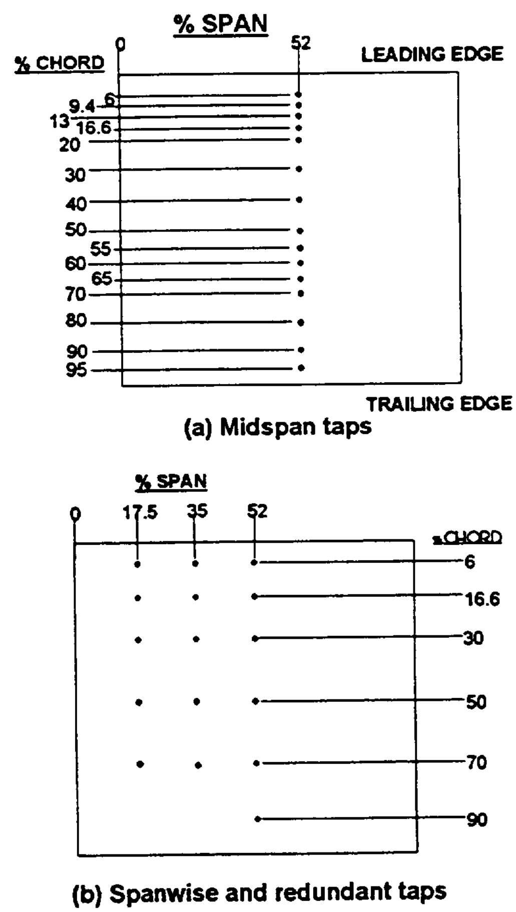

Fig. 5 Airfoil surface pressure taps

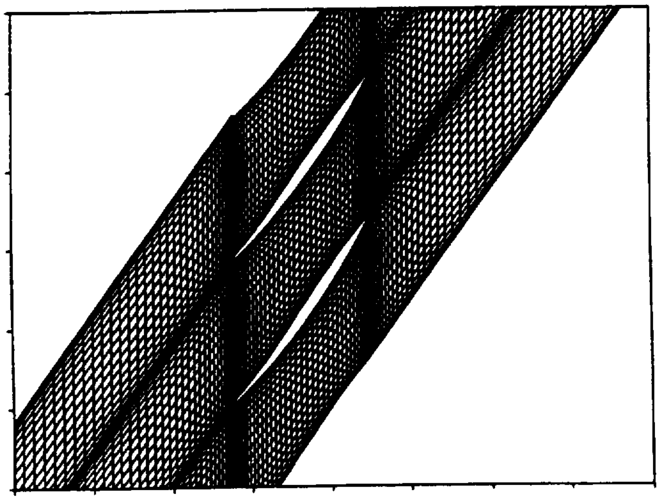

Fig. 6 SFLOW/LINFLO Grid

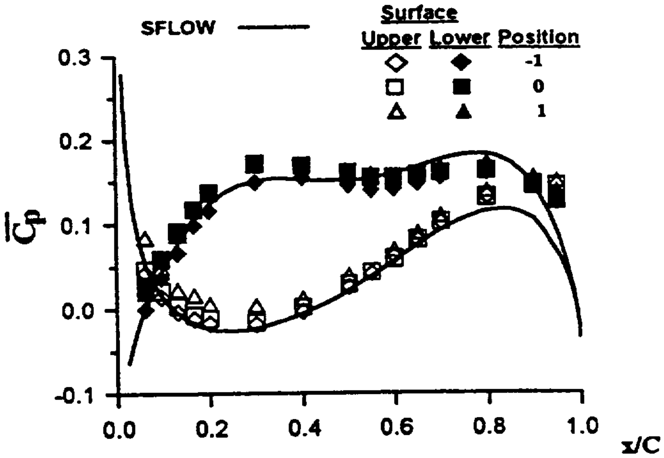

Fig. 7 Airfoil surface pressure coefficient distribution, M=0.2, α=0°

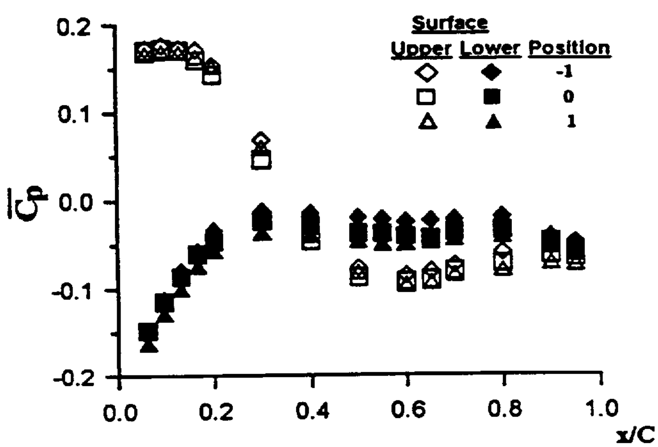

Fig. 8 Airfoil surface pressure coefficient distribution, M=0.2, α=10°

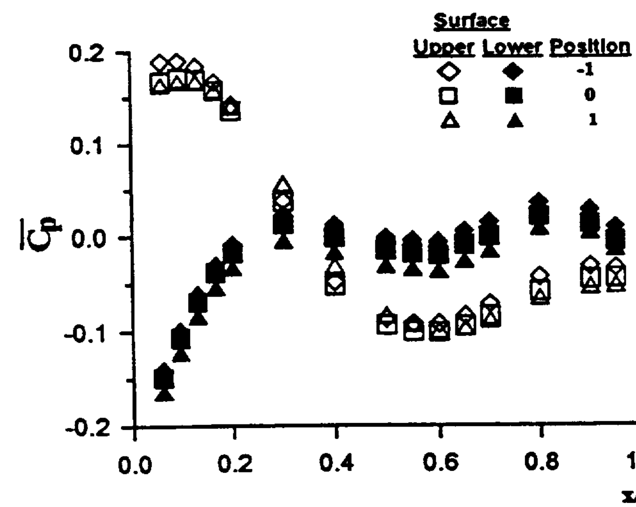

Fig. 9 Airfoil surface pressure coefficient distribution, M=0.8, α=10°

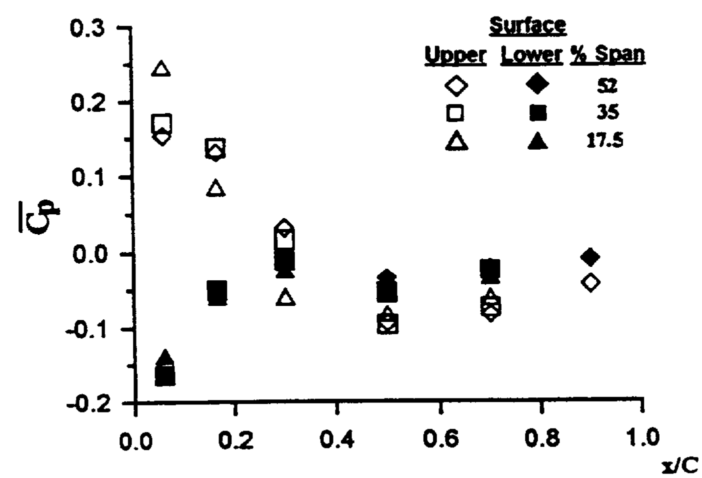

Fig. 10 Spanwise variation of airfoil surface pressure coefficient distribution, M=0.8, α=10°

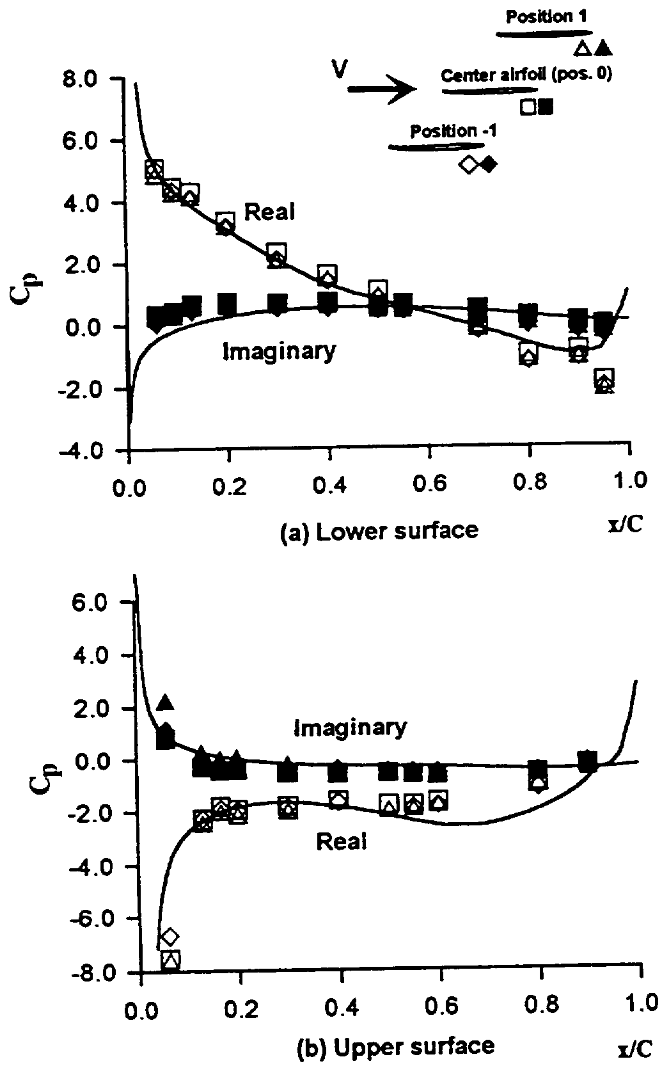

Fig. 11 First harmonic airfoil surface pressure coefficients, M=0.2, α=0°, β=180°, k=0.8

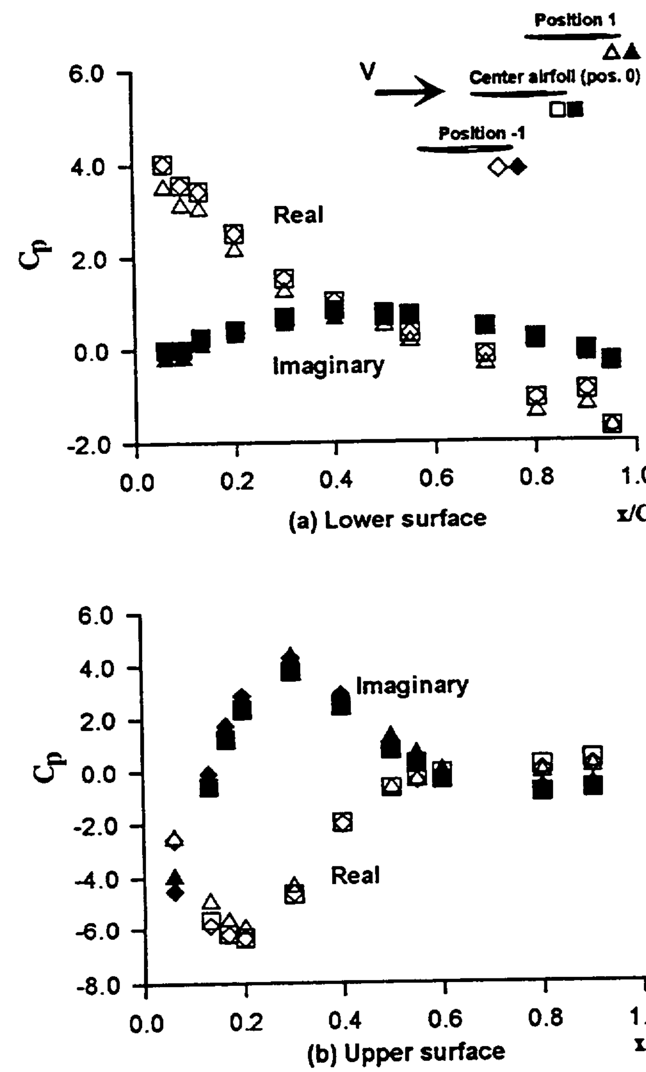

Fig. 12 First harmonic airfoil surface pressure coefficients, M=0.2, α=10°, β=180°, k=0.8

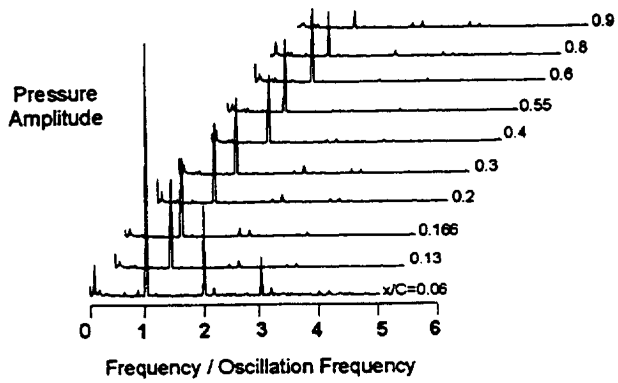

(a) α=0°

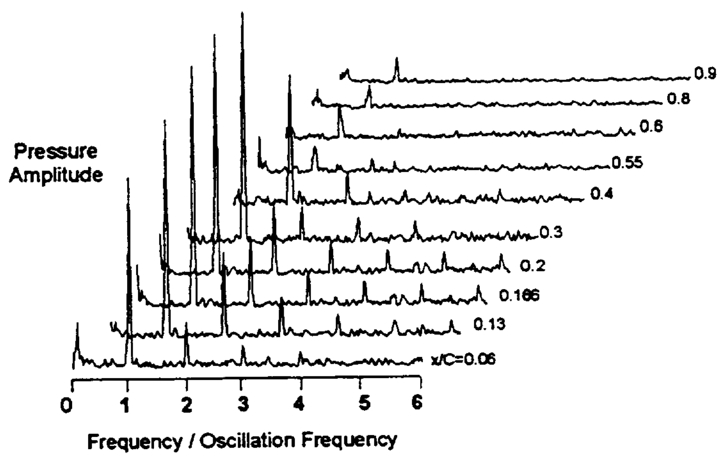

(b) α=10°

Fig. 13 Airfoil upper surface pressure spectra, M=0.2, β=180°, k=0.8

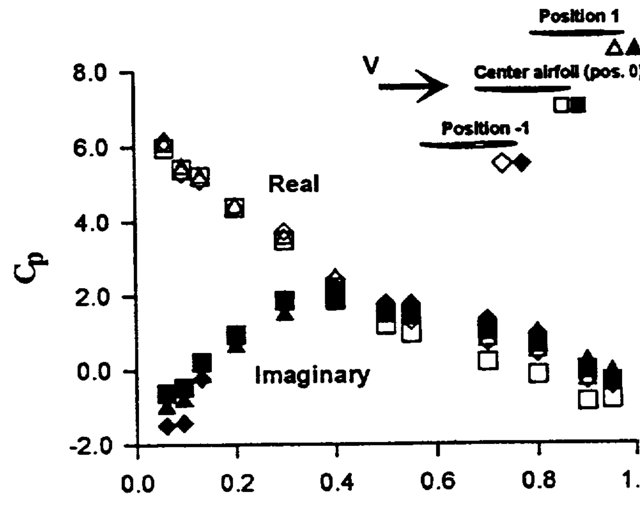

(a) Lower surface

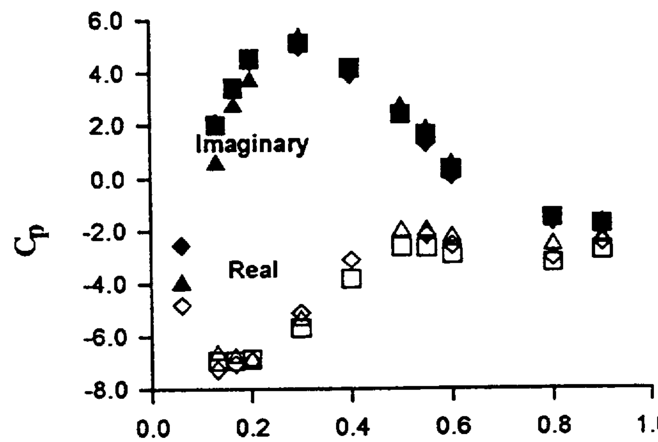

(b) Upper surface

Fig. 14 First harmonic airfoil surface pressure coefficients, M=0.8, α=10°, β=180°, k=0.4

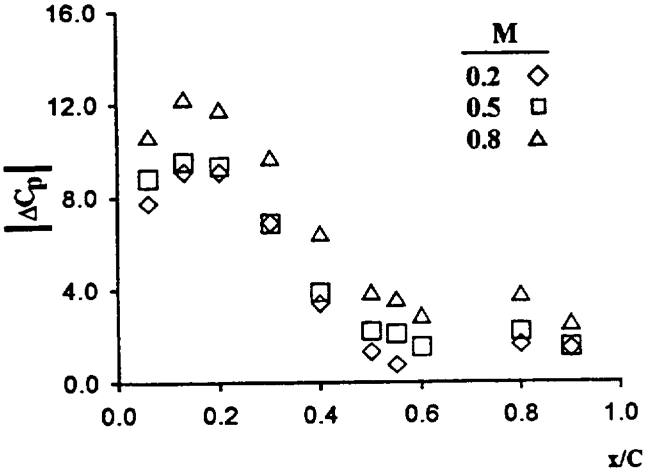

(a) Magnitude

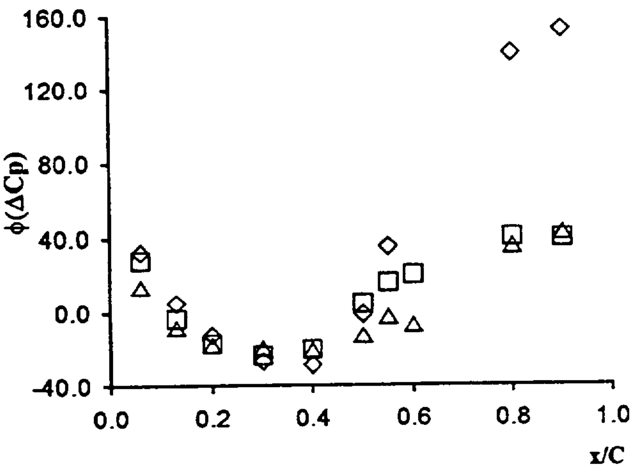

(b) Phase

Fig. 15 Effect of Mach number on unsteady pressure difference coefficient, $\alpha = 10°$, k=0.8

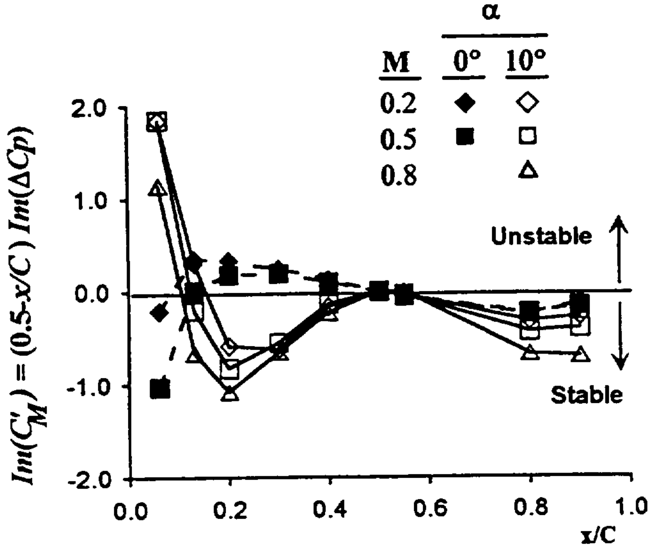

Fig. 16 Effect of incidence and Mach number on chordwise distribution of unsteady aerodynamic work/cycle, k=0.8

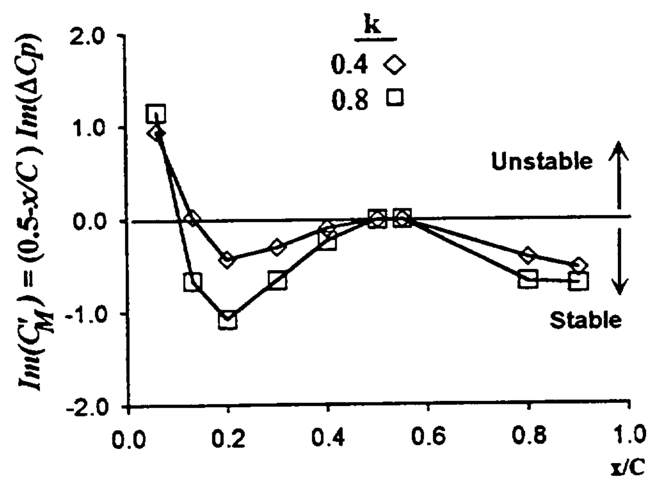

Fig. 17 Effect of reduced frequency on chordwise distribution of unsteady aerodynamic work/cycle, M=0.8

REPORT DOCUMENTATION PAGE

Form Approved
OMB No. 0704-0188

1. AGENCY USE ONLY (*Leave blank*)	2. REPORT DATE	3. REPORT TYPE AND DATES COVERED
	July 1996	Technical Memorandum

4. TITLE AND SUBTITLE

Experimental Investigation of Unsteady Flows at Large Incidence Angles in a Linear Oscillating Cascade

5. FUNDING NUMBERS

WU–505–62–10

6. AUTHOR(S)

Daniel H. Buffum, Vincent R. Capece, Aaron J. King, and Yehia M. EL-Aini

7. PERFORMING ORGANIZATION NAME(S) AND ADDRESS(ES)

National Aeronautics and Space Administration
Lewis Research Center
Cleveland, Ohio 44135–3191

8. PERFORMING ORGANIZATION REPORT NUMBER

E–10358

9. SPONSORING/MONITORING AGENCY NAME(S) AND ADDRESS(ES)

National Aeronautics and Space Administration
Washington, D.C. 20546–0001

10. SPONSORING/MONITORING AGENCY REPORT NUMBER

NASA TM–107283
AIAA–96–2823

11. SUPPLEMENTARY NOTES

Prepared for the 32nd Joint Propulsion Conference cosponsored by AIAA, ASME, SAE, and ASEE, Lake Buena Vista, Florida, July 1–3, 1996. Daniel H. Buffum, NASA Lewis Research Center; Vincent R. Capece and Aaron J. King, University of California, Department of Mechanical and Aeronautical Engineering, Davis, California 95616; Yehia M. EL-Aini, Pratt & Whitney, West Palm Beach, Florida. Responsible person, Daniel H. Buffum, organization code 2760, (216) 433–3759.

12a. DISTRIBUTION/AVAILABILITY STATEMENT

Unclassified - Unlimited
Subject Category 07

This publication is available from the NASA Center for AeroSpace Information, (301) 621–0390.

12b. DISTRIBUTION CODE

13. ABSTRACT ***(Maximum 200 words)***

The aerodynamics of a cascade of airfoils oscillating in torsion about the midchord is investigated experimentally at a large mean incidence angle and, for reference, at a low mean incidence angle. The airfoil section is representative of a modern, low aspect ratio, fan blade tip section. Time-dependent airfoil surface pressure measurements were made for reduced frequencies up to 0.8 for out-of-phase oscillations at Mach numbers up to 0.8 and chordal incidence angles of 0° and 10°. For the 10° chordal incidence angle, a separation bubble formed at the leading edge of the suction surface. The separated flow field was found to have a dramatic effect on the chordwise distribution of the unsteady pressure. In this region, substantial deviations from the attached flow data were found with the deviations becoming less apparent in the aft region of the airfoil for all reduced frequencies. In particular, near the leading edge the separated flow had a strong destabilizing influence while the attached flow had a strong stabilizing influence.

14. SUBJECT TERMS

Cascade; Unsteady aerodynamics

15. NUMBER OF PAGES	16. PRICE CODE
15	A03

17. SECURITY CLASSIFICATION OF REPORT	18. SECURITY CLASSIFICATION OF THIS PAGE	19. SECURITY CLASSIFICATION OF ABSTRACT	20. LIMITATION OF ABSTRACT
Unclassified	Unclassified	Unclassified	